New Insights into Computational Fluid Dynamic Modeling of the Resistivity and Overpotential in Reverse Electrodialysis

Zohreh Jalili[a,b], Odne Stokke Burheim[b] and Kristian Etienne Einarsrud[a]

[a]Department of Materials Science and Engineering, Norwegian University of Science and Technology (NTNU), Trondheim 7491, Norway

[b]Department of Energy and Process Engineering, Norwegian University of Science and Technology (NTNU), Trondheim 7491, Norway

The resulting electrical potential of a reverse electrodialysis is reduced both due to ohmic and non-ohmic resistances. The non-ohmic resistance is mainly controlled by concentration polarization which is a considerable challenge in a membrane based processes and is a result of accumulation or depletion of specific ions adjacent to the ionic exchange membranes compared to the bulk solution. This phenomenon effectively reduces the driving force across the membrane, hence affects the performance of the process. The present work aims to present a numerical model based on coupled Navier-Stokes and Nernst-Planck equations to predict flow and pressure drop as well as concentration and electrical potential for optimizing the performance of the system, using OpenFOAM. The model is demonstrated in a flat and spacer-filled channel for different Reynolds number. The results reveal that reducing the Reynolds number and introducing flow promoters such as cylindrical corrugations in a dilute solution channel reduces the resistivity of a RED unit cell, hence increasing the produced electrical potential. However, introducing cylindrical corrugations in a concentrated solution channel has an adverse effect on the resistivity, leading to an unfavorable resistivity increment.

Introduction

Salinity gradient energy (SGE) is a promising source of sustainable energy and is obtained by mixing two aqueous solutions with different salinity (for example river and sea water), applying membrane based technologies such as pressure retarded osmosis (PRO), reverse electrodialysis (RED) or capacitive mixing (CAPMIX) (1, 16–19, 24, 29, 30). The coupling of these technologies for energy generation to their corresponding desalination technologies can establish a concentration battery (1), for example recently Kingsbury et al. (3) proposed a concentration battery by coupling of electrodialysis (ED) and reverse electrodialysis (RED). During charging of a ED/RED battery, ions move from the dilute solution towards the concentrated solution through ED, and during discharging by RED, the electrical current is reversed and ions move back from the concentrated to the dilute solution, restoring the initial condition. A schematic of a RED stack is shown in Figure 1. The stack consists of series of channels separated by ion-selective membranes. Concentrated and dilute solutions are pumped through these channels. Anion exchange membranes (AEM) are used to let anions transport and cation exchange membranes (CEM) are used to let cations transport; thus an ionic

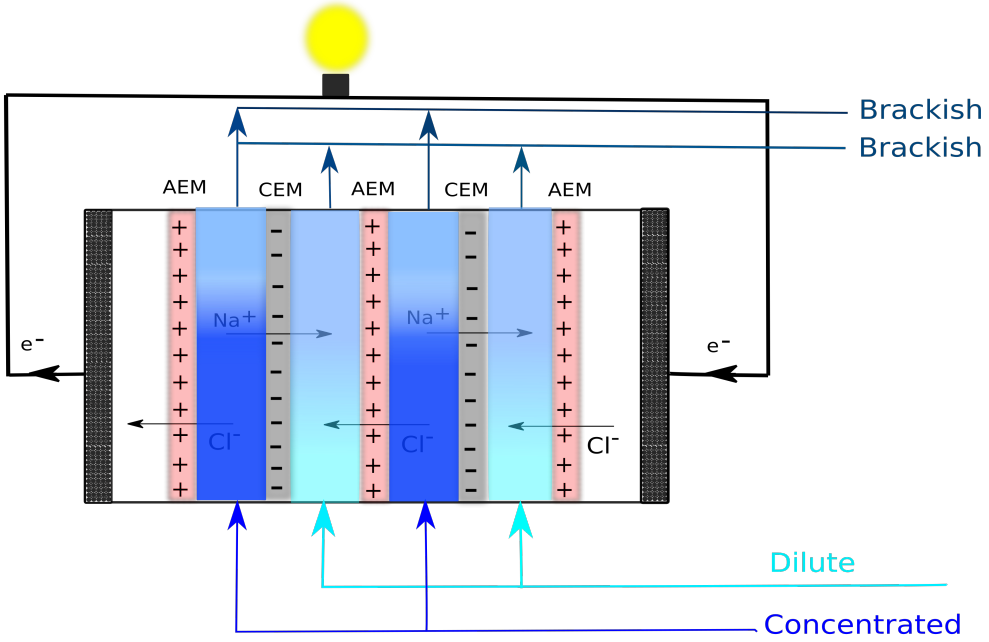

Figure 1. Schematic of a RED stack.

current will be established between the concentrated and dilute solutions. Polyvalent salts such as $FeCl_2$ and $FeCl_3$ are the two electrode rinse solutions at both ends of the stack for redox reaction to convert the ionic flux to electrical current and harvesting an ionic current to power an external load (25–27). The open circuit potential for a unit cell depends on the concentration of concentrated and dilute solutions, temperature and the perm-selectivity of the two membranes, described by Equation 1 (2, 16):

$$E_{OCP} = 2\frac{\overline{\beta}RT}{F}\ln\left(\frac{C_c}{C_d}\right), \quad [1]$$

where C_c and C_d are concentrations of the concentrated and dilute solutions, respectively. F is Faraday's constant, T is temperature, R is the universal gas constant and $\overline{\beta}$ is the average perm-selectivity. Due to the resistivity of the unit cell, the produced voltage from the unit cell is lower than E_{OCP} and decreases as electrical current increases. In fact, this potential decrease is due to both ohmic loss, concentration change in the boundary layer and concentration change in the bulk of the solution. Potential drop due to concentration change in the boundary layer and concentration change in the bulk of the solution can be interpreted as non-ohmic potential loss (2). In other words, non-ohmic resistance can be calculated by dividing of the non-ohmic potential loss by the current density. The produced potential of the unit cell can be expressed as follows (2):

$$E_{unit\ cell} = E_{OCP} - r_{ohmic}j - r_{non\text{-}ohmic}j, \quad [2]$$

where, r_{ohmic} is the ohmic area resistance ($\Omega.m^2$) and $r_{non-ohmic}$ is the non-ohmic area resistance ($\Omega.m^2$). If there is no current, the produced potential of the system is equal to the open circuit potential (E_{OCP}), and can be calculated according to Equation 1. The

ohmic area resistance of the unit cell can be calculated by the Equation 3 (2, 16):

$$r_{unitcell} = \left(\frac{r_{AEM}}{1-\sigma} + \frac{r_{CEM}}{1-\sigma} + \frac{h_c}{\varepsilon^2 \cdot k_c} + \frac{h_d}{\varepsilon^2 \cdot k_d} \right), \quad [3]$$

where r_{AEM} and r_{CEM} are the area resistance of the AEM and CEM, respectively. σ is the mask fraction or the shadow factor of non-conductive spacers (2) and ε is the spacer porosity, h_d and h_c are the heights of the dilute and concentrated solutions compartments, k_c and k_d are the concentrated and dilute solutions conductivities, respectively. The maximum power density (W/m^2) of the RED unit cell is calculated as below:

$$P_{RED}^{max} = \frac{1}{r_{unit\ cell}} \frac{{E_{OCP}}^2}{4}. \quad [4]$$

Another source of power loss during energy generation by membrane based technologies is concentration polarization. During the ion transport through the membranes, ion concentration near the membrane-dilute solution interface increases compared to the dilute bulk concentration and ion concentration adjacent to the membrane-concentrated solution interface decreases compared to the concentrated bulk concentration, therefor a thin diffusion boundary layer (DBL) along the ion exchange membranes will be established. Accordingly, the driving force is related to the concentration difference across the membrane surface which is smaller than the bulk concentration difference between the two streams; hence this results in reducing the performance of the process compared to the theoretical value. This phenomenon is known as concentration polarization (4, 5, 8, 9). Concentration polarization has been discussed extensively in the literature (4, 6–8). The concentration polarization effect is also sometimes referred as non-ohmic resistance (8). In fact, non-ohmic resistance is both due to diffusion boundary layer resistance and electrical double layer resistance. However, since the thickness of electrical double layer is significantly lower than the thickness of diffusion boundary layer, non-ohmic resistance is controlled mainly by diffusion boundary layer resistance (28). Increasing the flow velocity (Reynolds number) and introducing the flow promoters (i.e. spacers) can mitigate the concentration polarization and enhance the mass transfer in membrane-based processes by disturbing the diffusive boundary layer (4, 7, 10, 11). Vermaas et al. experimentally measured the power density obtained by RED and assessed the role of Re number on the ohmic and non-ohmic resistances for channel designs with and without mixing promoters (23). They documented that a RED stack should operate with small distance between the membranes and at low flow rates to obtain higher power density with lower pump power consumption (23). Equation 3 shows that the distance between the membranes (channel height) has to be reduced particularly for dilute compartment to reduce the resistivity of the stack, since the conductivity of dilute solution is lower than concentrated solution. However at low flow rates, the diffusive boundary layer near the membranes and concentration polarization are considerable; i.e. the non-ohmic resistance is significant. Vermaas et al. demonstrated that how the non-ohmic resistance in RED can be reduced (resulting to increase the power density) without increasing the power consumption significantly (23). They showed also that while the ohmic resistance is almost independent of the Re number at high Re numbers, the non-ohmic resistance decreases significantly by increasing the Reynolds number (23). In addition, the ohmic resistance was reported much higher than non-ohmic resistance for all range of Reynolds numbers and therefore the ohmic resistance dominates the power loss. Their observations showed that at the low Re numbers which are typically used for RED, using of the corrugations

are not that beneficial (23). In practice, the spacers keep the ions selective membranes separated in a RED stack. Spacers can be ion conductive or non-conductive. Dlugolecki et al. documented that non-conductive spacers create a spacer shadow effect by hindering of ionic transport from the membrane to the solution, resulting to reduce the available membrane area and increase the ohmic stack resistance (10). They used ion-conducive spacers to omit spacer shadow effect and enhance the power generation. They compared theoretical stack resistance and power density of ion-conductive and non-conductive spacers at different Re numbers (10). Dlugolecki et al. reported that applying commercially available conductive spacer increases the power density in RED around 30 to 40% and reduces the resistivity of stack around 20% compared to non-conductive spacers, considering the same geometry (10). They observed also that by increasing the flow velocity, concentration polarization reduces and the gross power density increases (10).

Experimental investigation of mass and momentum transport as well as potential drop during RED demands time and considerable cost. Computational fluid dynamic (CFD) is a good alternative. While several studies have been reported to apply CFD modeling for investigating momentum and mass transfer to find a trade-off between the pressure loss and mass transfer in a RED channel (4, 6, 9–11, 15, 15), there are limited studies of electrical potential drop in a RED channel. The interaction between ionic species and fluid flow can be achieved by solving the coupled Navier-Stokes (NS) and Nernst-Planck (NP) equations (11, 15), allowing for simultaneous prediction of flow and pressure fields, concentration and electrical potential, all of which are of interest for the overall performance of the system. Lacey utilized the Nernst equilibrium equation to calculate the potential of a RED unit cell with flat channels by assuming a constant boundary layer thickness to obtain the linear concentration profile along the compartments, analytically (12). Sonin and Probstein also applied Nernst-Planck (NP) equation to calculate the potential of a ED unit cell with flat channels by assuming fully developed (parabolic profile) concentration profile (22).

The current work describes a numerical framework for simulation of Navier-Stokes (NS) and Nernst-Planck (NP) system based on the open source CFD platform OpenFOAM (20), aiming to predict the influence of flow velocity (by varying Re number from 1-100) and geometry (flat channel versus cylindrical non-ion conductive spacer-filled channel) on concentration, pressure drop and electrical potential drop. The numerical result for a flat channel has been verified by comparing the calculated electric potential drop with an analytical solution proposed by Lacey (12) for both dilute and concentrated channels. The current simulation framework dose not require given concentration profile and diffusive boundary layer thickness, as many previous models needed (12, 22). The influence of Re number and corrugation on the total resistance of the unit cell (ohmic and non-ohmic resistances), pressure loss as well as electric potential for both dilute and concentrated channels will be addressed.

Model description

This section is divided into three subsections. First, the characteristics of the two studied geometries of the channels are illustrated and explained. Second, governing equations for CFD modeling and associated boundary conditions are described. Finally, the methodology to perform simulation modeling was discussed.

Geometry

A flat channel and a non-ion conductive spacer-filled channel with cylindrical corrugation are investigated for both concentrated and dilute solutions. Figure 2 shows a schematic of the two studied geometries with characteristic lengths.

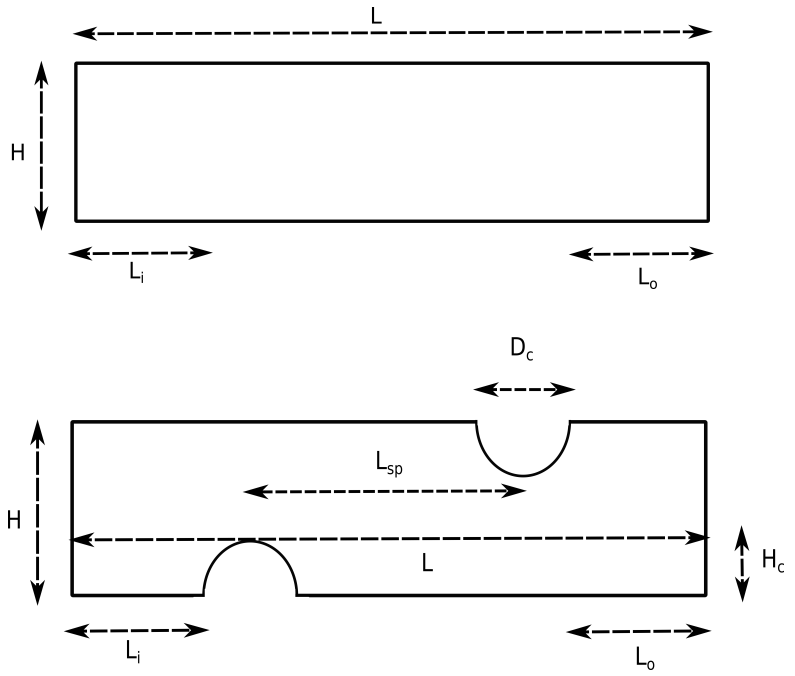

Figure 2. Schematic of the geometry of flat channel and the cylindrical corrugated channel.

In this figure, H is the height of the channel. The channel includes a small inactive upstream section with length L_i (for both top and bottom walls) in order to remove any entrance effects on the flow before entering the active membrane section. L_{sp} is the distance between the centre of two successive corrugations. An inactive downstream section with the length of L_o (for both top and bottom walls) is introduced at the end of the channel to ensure that the created wakes in the downstream of the last corrugation at high Re numbers is far enough from the outlet boundary to prevent any instability due to back flow at the outlet. The corresponding values of the parameters for each geometry is given in Table I.

TABLE I. Characteristic parameters of the studied geometries

Parameter	Symbol	Value (mm)
Corrugation diameter	D_c	0.1
Length of the channel	L	7.2
Height of the channel	H	0.2
Number of corrugations	N	16 (dimensionless)
Height of the corrugation	H_c	0.05
Length of inlet or outlet section	L_i, L_o	0.55
Distance of two successive corrugations centre	L_{sp}	0.4

Mathematical model

The flow in the channel is assumed to be 2-dimensional ($\vec{u}(x,y)$), steady and laminar and physical properties such as density and viscosity are assumed to be constant, for

given concentrations. The flow between the membranes is governed by the continuity equation,

$$\nabla \cdot \vec{u} = 0, \tag{5}$$

and the incompressible Navier-Stokes equations:

$$\rho \vec{u} \cdot \nabla \vec{u} = -\nabla p + \mu \nabla^2 \vec{u}. \tag{6}$$

The solutions are assumed to be governed by dilute solution theory with activity coefficients of order unity and the solution is thus fully described by its concentration.

The transport of ions is governed by the Nernst-Plank equation(13, 14, 22), under the current assumptions given as:

$$\nabla \cdot [\mathcal{D}_i \nabla C_i - \vec{u} C_i + C_i \mu_{EP} \nabla \phi] = 0, \tag{7}$$

for specie i where C_i is the concentration ([mol/m^3]), $\mathcal{D}_i$ is the diffusivity ([m^2/s]), $\vec{u}$ is the fluid velocity ([m/s]),

$$\mu_{EPi} = \frac{\mathcal{D}_i z_i F}{RT} \tag{8}$$

is the electrophoretic mobility ([m^2/Vs]) where z_i is the valency and ϕ is the electrostatic potential ([V]).

Assuming two ionic species, denoted + and -, we thus have two transport equations;

$$(\vec{u} \cdot \nabla) C_+ = \nabla \cdot (\mathcal{D}_+ \nabla C_+) + \nabla \cdot (C_+ \frac{\mathcal{D}_+ z_+ F}{RT} \nabla \phi) \tag{9}$$

and

$$(\vec{u} \cdot \nabla) C_- = \nabla \cdot (\mathcal{D}_- \nabla C_-) + \nabla \cdot (C_- \frac{\mathcal{D}_- z_- F}{RT} \nabla \phi). \tag{10}$$

Introducing the non-dimensional potential:

$$\tilde{\phi} = \frac{F\phi}{RT}, \tag{11}$$

assuming charge neutrality ($C_+ = C_- = C$) and monovalent ions ($z_+ = 1, z_- = -1$), equations 9 and 10 simplify to

$$(\vec{u} \cdot \nabla) C = \nabla \cdot (\mathcal{D}_+ \nabla C) + \nabla \cdot (C \mathcal{D}_+ \nabla \tilde{\phi}) \tag{12}$$

and

$$(\vec{u} \cdot \nabla) C = \nabla \cdot (\mathcal{D}_- \nabla C) - \nabla \cdot (C \mathcal{D}_- \nabla \tilde{\phi}). \tag{13}$$

Multiplication of Equation 12 with $\mathcal{D}_-$, Equation 13 with $\mathcal{D}_+$ and adding them together, assuming constant diffusivities, yields

$$\mathcal{D}_- \cdot (\vec{u} \cdot \nabla) C + \mathcal{D}_+ \cdot (\vec{u} \cdot \nabla) C = 2 \cdot \mathcal{D}_+ \cdot \mathcal{D}_- \cdot \nabla^2 C \tag{14}$$

$$\rightarrow (\vec{u} \cdot \nabla) C = \frac{2 \cdot \mathcal{D}_+ \cdot \mathcal{D}_-}{\mathcal{D}_+ + \mathcal{D}_-} \nabla^2 C \equiv \mathcal{D} \nabla^2 C, \tag{15}$$

where $\mathcal{D}$ is an effective diffusivity for the salt. Evidently, the *governing equation* for the concentration is decoupled from the electrical potential under the given conditions, thus simplifying the system of equations to be solved.

Owing to the assumptions of constant physical parameters (e.g. density and viscosity), the flow equations are decoupled from those governing the concentration, allowing for the former to be solved independently of the latter. With known concentration profiles, the electrical potential can be determined from the conservation of electrical current density $\vec{j}$,

$$\nabla \cdot \vec{j} = 0. \qquad [16]$$

The electrical current density can be determined by the flux of the species;

$$\begin{aligned} \vec{j} &= F\sum_i z_i N_i = F\sum_i z_i \left(\mathcal{D}_i \nabla c_i - u c_i + c_i \frac{\mathcal{D}_i z_i F}{RT} \nabla \phi \right) \\ &= F\left(\mathcal{D}_- - \mathcal{D}_+ \right) \nabla c - Fc\left(\mathcal{D}_+ + \mathcal{D}_- \right) \nabla \tilde{\phi} \end{aligned} \qquad [17]$$

Introducing the follwoing substitution:

$$\delta_{\mathcal{D}} = \frac{\mathcal{D}_+ - \mathcal{D}_-}{\mathcal{D}_+ + \mathcal{D}_-} \qquad [18]$$

and invoking Equation 16, one finally obtains:

$$-\delta_{\mathcal{D}} \nabla^2 c = \nabla \cdot \left(c \nabla \tilde{\phi} \right) \qquad [19]$$

Boundary condition

The inlet of the domain is specified with uniform concentration with the value of 0.016 *molar* (close to the typical salinity of brackish water which is around 0.015 *molar*), for the dilute solution channel and value of 0.484 *molar* (close to the average salinity of seawater which is around 0.6 *molar*), for the concentrated solution channel. Figure 3 shows the specified boundary conditions for different parts of the channel. A constant flux is assumed on the membrane surface, given by:

$$\mathrm{j}_w = -\mathcal{D} \left. \frac{\partial C}{\partial n} \right|_w , \qquad [20]$$

where n is the wall normal direction and $\mathcal{D}$ is the effective diffusivity, representative of the ionic flux through the membrane.

The value of the velocity at the inlet depends upon the sought Reynolds number, and is given as parabolic profile. The outlet is specified to atmospheric pressure. The membranes and spacers set to no-slip condition at walls with zero gradient in pressure. In the case of the spacer-filled channel, the spacers are assumed non-ion conductive, with a corresponding zero flux boundary condition. The electric potential at the bottom wall of the channel is set to zero and the electrical potential on the top wall (active membrane) will be calculated based on the Equation 17 applying the current density (A/m^2) at maximum power density of the unit cell, as specified in Table II:

TABLE II. Input values for current densities for flat and cylindrical spacer-filled channels

E_{OCP} (volt)	T (K)	A_{flat} (m^2)	$A_{cyl.}$ (m^2)	r (ohm.m ^{2})	I (A)	j_{flat} (A/m^2)	$\mathrm{j}_{cyl.}$ (A/m^2)
0.176	300	6.4×10^{-07}	5.6×10^{-07}	0.00144	3.66×10^{-05}	57	65

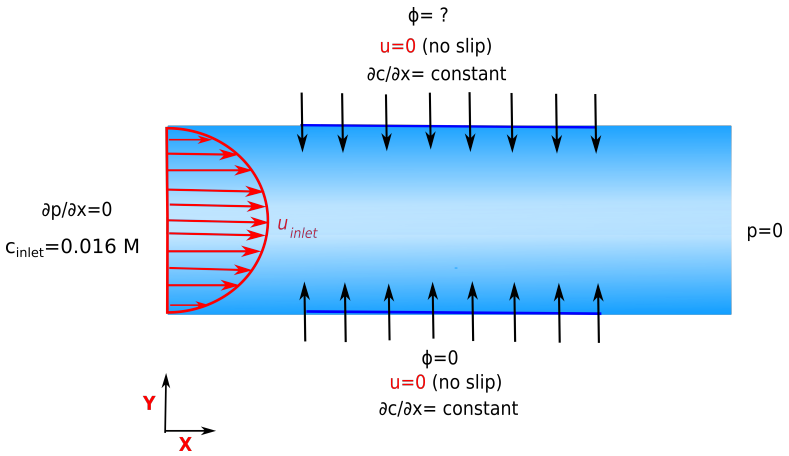

Figure 3. The boundary conditions for a dilute flat channel. The blue line shows the active membrane section, and the arrows show the diffusion direction from the top and bottom wall toward the dilute bulk.

The spacers (cylindrical corrugations) are not active in terms of transporting ions hereupon, the current densities for a flat and corrugated channel will be different due to different available membrane area. In spite of having same current in both configurations, the different current densities will be set to different geometries to keep the comparison logical.

Methodology

OpenFOAM version 4.1 (20) is used for CFD simulation modeling. The simulation studies were performed on a small cluster running CentOS 7.4 with 4 Xeon E5-2650 CPUs running at 2.2 GHz equipped with 128 Gb RAM. Details regarding the schemes and solvers present in OpenFOAM can be found elsewhere (20). Navier-Stokes, continuity, and Nernst-Planck equations were solved at steady-state condition with a newly developed steady state in-house solver. This solver is developed based on the SIMPLE algorithm to calculate the decoupled concentration and electrical potential. The utility groovy BC (21) is utilized to set the parabolic velocity in the inlet of the channel and the boundary conditions for electrical potential as described by Equation 17. The utility funkySetFields (21) is used to set linear concentration profile as boundary condition to verify the numerical model with analytical solution proposed by Lacey (12).

Results and Discussion

Verification

The purpose of this section is to verify the numerical model with the analytical solution that proposed by Lacey with assuming a constant boundary layer thickness and obtaining the linear concentration profile along the compartments (12) to estimate the potential of a RED unit cell with flat channel. Figure 4 shows the concentration and the corresponding electrical potential across the height of the dilute compartment for a linear concentration profile based on Lacey and numerical solution of our model. The potential changes linearly versus the height of the channel for a constant concentration profile, since there is no concentration polarization in the dilute bulk solution. When the concentration profile is varying linearly across the height of the channel at diffusive

boundary layer, the potential becomes a logarithmic function. The figure illustrates that results estimated by numerical model is in good correspondence with the analytical solution.

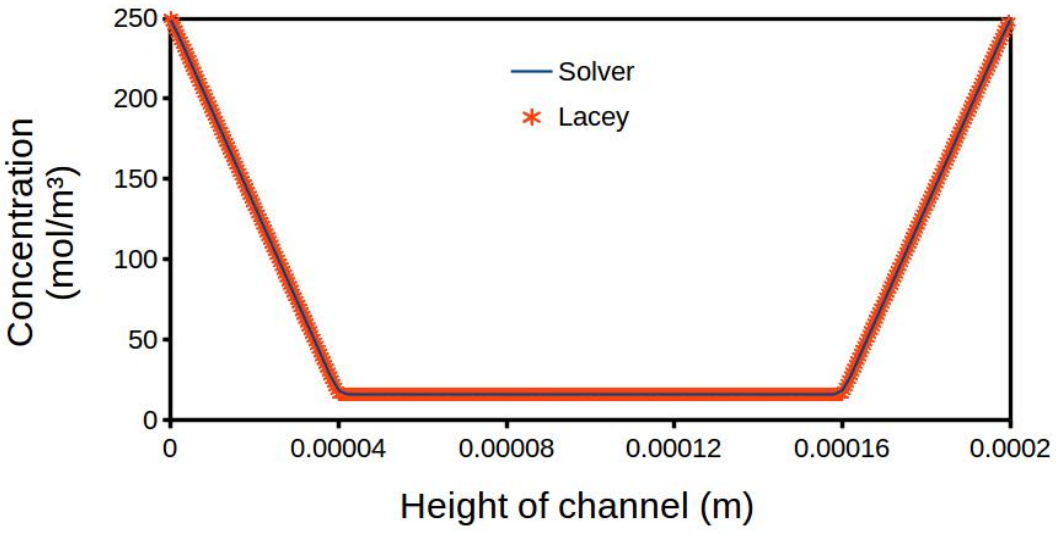

(a)

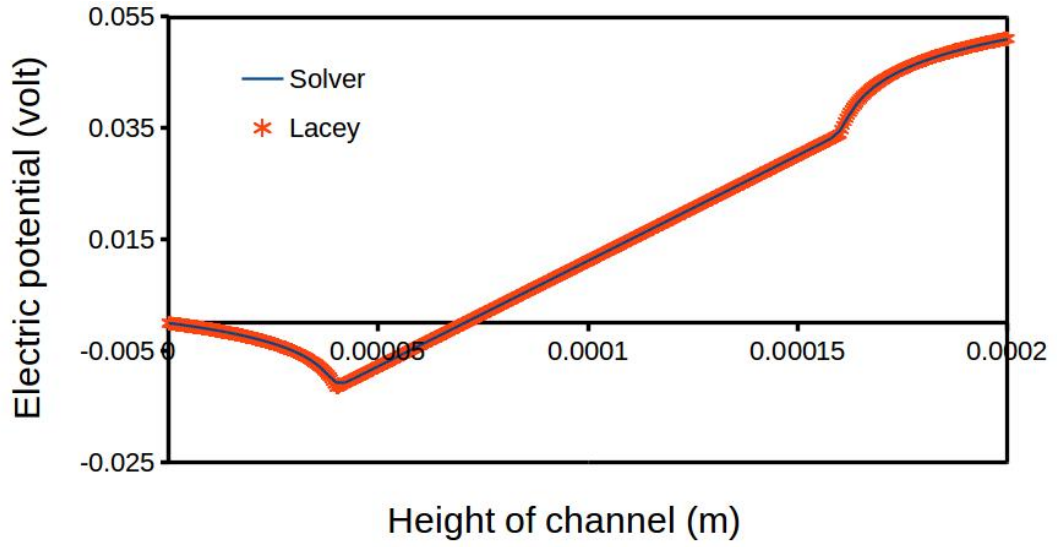

(b)

Figure 4. Concentration and the corresponding potential distribution across the height of a flat channel from Lacey's analytical model and our numerical simulation. (a) The concentration profile (b) The corresponding electric potential with j= 77.9 A/m^2.

Influence of velocity and corrugations on pressure loss and total resistivity

The purpose of this subsection is to investigate the effect of Re number and corrugations on the ohmic and non-ohmic resistivity of dilute or concentrated solution compartments and pressure loss. Figure 5 demonstrates the concentration profiles versus the height of the flat channel at different Reynolds numbers (1, 40 and 100) at the specific distance from the inlet (X = 0.005 m) for concentrated and dilute solutions. Two observations can be extracted from this figure. First, the concentration at the center of the channel is at maximum and minimum values compare to the concentration near the

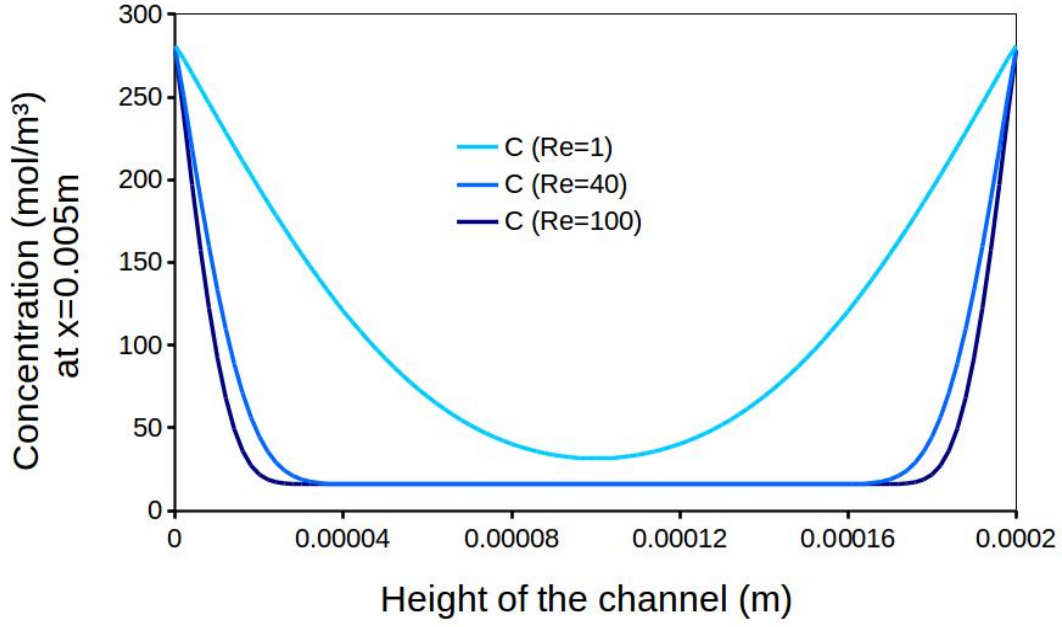

(a)

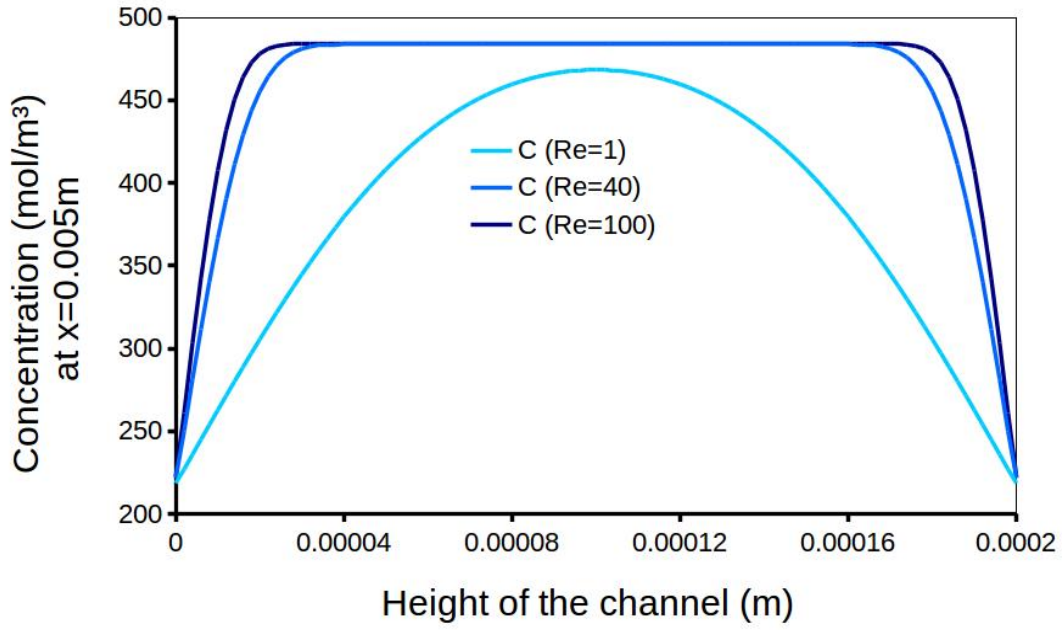

(b)

Figure 5. Concentration profiles versus the height of the flat channel at different Reynolds numbers (1, 40 and 100) at X = 0.005 m from inlet (a) dilute solution, (b) concentrated solution.

walls of the channel for concentrated and dilute compartments, respectively. Second, as Re number increases, the concentration gradient near the walls of the channel increases due to reducing of the boundary layer thickness by increasing Re number and enhancing advection mechanism.

Analysis of pressure drop versus Re number for a flat channel and cylindrical spacer filled-channel revealed that flat channel has the lower pressure drop compare to cylindrical corrugation as shown by Figure 6a. The pressure loss difference between cylindri-

cal spacer filled-channel and flat channel enhances drastically as Re number increases from 40 to 100. The figure also shows that the pressure drop for concentrated solution is higher than dilute solution for similar geometry and Re number due to density difference between the two solutions. Similar observation was reported in experiments conducted by Zhu et al. (28).

The total resistance of a RED stack is sum of ohmic and non-ohmic resistances, as discussed previously. In this work, the total area resistance of the dilute and concentrated solution compartments is calculated by dividing the area averaged potential for the top wall of the channel by the current density at maximum power density of RED unit cell, expressed by Equation 21:

$$r = \frac{1}{Aj} \int_{top\ wall} \phi \, dA, \qquad [21]$$

where A is the active membrane area on top wall of a flat or corrugated channel, and r is the total area resistance (ohmic and non-ohmic) of the concentrated or dilute compartments which is shown in Figure 6b for the concentrated solution (right vertical axis) and for the dilute solution (left vertical axis) as a function of Re number, for both flat channel and spacer-filled channel.

Three observations can be extracted from this figure. First, the resistance of dilute solution is significantly larger the resistance of concentrated solution for a given Re number and channel geometry, i.e. the resistance of the dilute solution controls the resistivity of a RED stack and should be reduced to achieve higher net power output. Second, introducing corrugations in a dilute solution channel reduces the resistivity through wakes down stream of corrugations. The velocity streamlines are shown for a cylindrical spacer-filled channel in Figure 7, when Re number is equal to 1 and 100. The figure demonstrates that for a higher Reynolds numbers, the streamline pattern in the down stream of corrugations are changing and wakes are developing, Figure 5. Third, as the thickness of the boundary layer decreases with increasing Re, the average concentration across the channel decreases for the dilute solution while it increases for the concentrated solution, thus the resistivity of the dilute solution increases by increasing Re number while resistivity of the concentrated solution decreases. This effect is stronger at lower Re, i.e. Re number less than 40. Similar observation is reported by Zhu et al. (28) that at lower velocities, the conductivity of dilute channels increases considerably due to enhanced transport of ions from concentrated solution into dilute solution. For high Re numbers (larger than 40), the variation of resistance for both dilute and concentrated solutions in a flat or cylindrical spacer-filled channel is small, since the concentration profiles for both dilute and concentration compartments are very similar for Re = 40 or Re = 100 (It is worth mentioning that the resistivity of concentrated solution is higher for cylindrical spacer filled-channel compared to a flat channel at a fixed Re number. Another interesting observation is related to the scale and magnitude of the variation of resistance for the dilute solution and concentrated solution, when Re number is increasing or geometry of channel is varying. For example, the resistivity of dilute solution for a flat channel increases for more than two times when Re number increases from 1 to 40, while the resistivity of concentrated solution decreases only by 15 %.

Considering Equation 2 and Figure 6b, the total resistivity of the unit cell can be reduced by decreasing the flow velocity and introducing corrugations in the dilute solu-

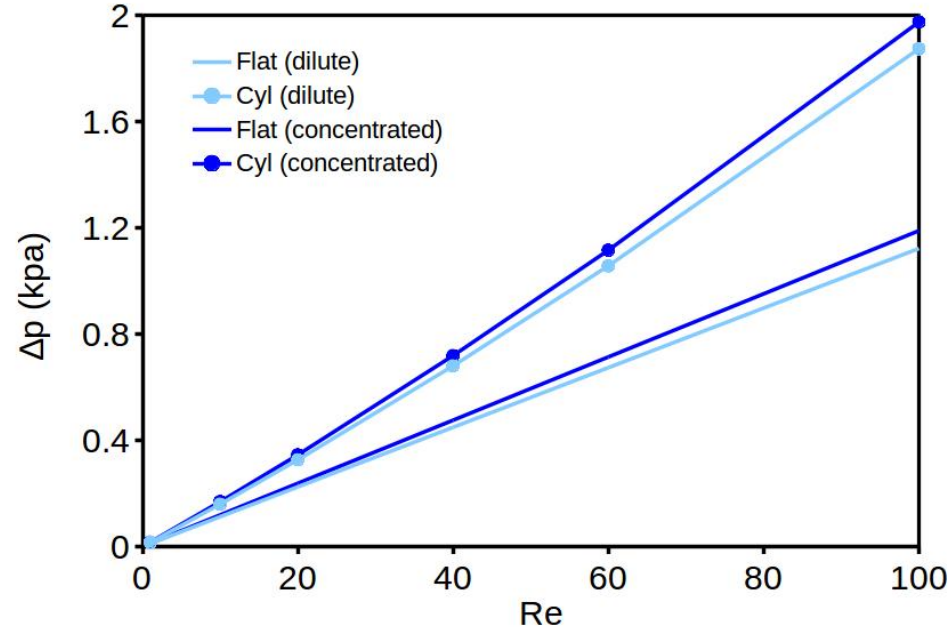

(a)

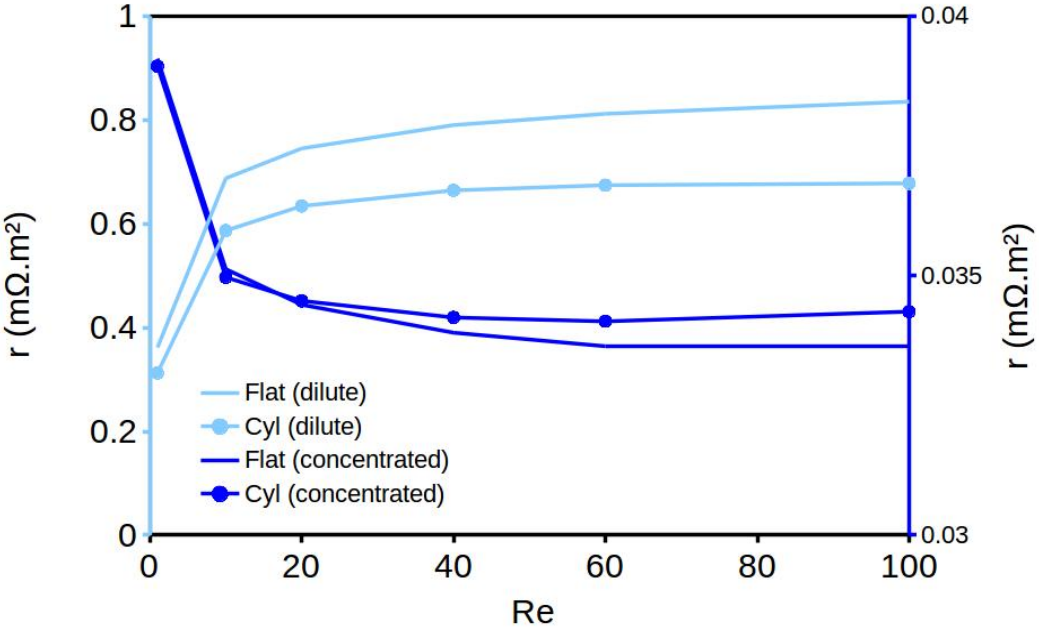

(b)

Figure 6. (a) Influence of Re number and geometry of channel on the pressure drop of the concentrated and dilute solution channels, (b) Influence of Re number and geometry of channel on the resistance of the concentrated and dilute solution channels.

tion stream. Decreasing the flow velocity may result to increasing of diffusion boundary layer resistance and accordingly one may find a trade off between decrease of dilute solution resistance and increasing of diffusion boundary layer resistance at low flow velocities as it is reported also by Zhu et al. (28). Increasing the flow velocity in concentrated solution stream will lead also to reduction of concentrated solution stream resistance but this reduction is not very strong.

It is important to highlight that introducing corrugations or increasing Re number

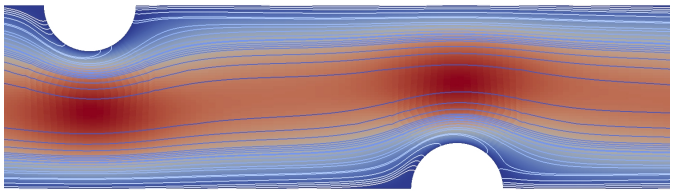

(a) Re=1

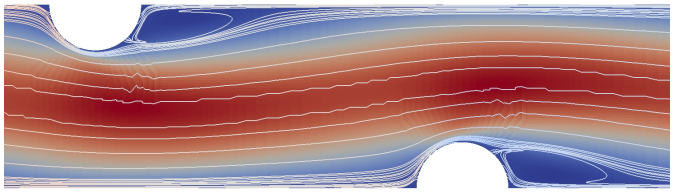

(b) Re=100

Figure 7. Streamlines of the velocity adjacent to the cylindrical corrugations and developed wakes for Re=100.

not only affect the resistivity of a RED stack but will influence also on the required energy for pumping of fluids in concentrated and dilute solutions. By increasing flow velocity and introducing promoters, the pressure loss of the flow through channel increases and one should find a balance between the mass flux enhancement and pressure loss to maximize energy generation from RED.

Considering both the effect of reducing the Re number on reducing resistivity of dilute solution and the pressure loss, one may conclude that reducing the flow rate in the dilute channel not only enhances the conductivity of the dilute channel (and thereby resistivity is reduced and the performance is improved), but will also lower the energy for pumping the solution. Increasing the Re number beyond 40 for the concentrated solution is not also that beneficial, since the change in resistance of concentrated solution channel is insignificant while the pressure loss is considerable.

Conclusion

The effect of flow velocities and geometry of channel on resistivity of concentrated and dilute solution channels in a reverse electrodialysis (RED) unit cell is addressed based on CFD modeling, enabling simulation of flow, pressure drop, concentration and electrical potential. The results show that the resistivity of dilute solution dominates the resistivity of concentrated solution for all range of studied Re number and for both flat channel and cylindrical spacer-filled channel. The produced electrical potential of a

RED unit cell improves by reducing the Re number and introducing flow promoters in a dilute solution channel, due to enhanced solution conductivity. Introducing cylindrical corrugations in a concentrated solution channel or increasing the flow velocity in a dilute solution channel have an adverse effect on produced electrical potential due to increasing resistivity. Therefore optimum flow velocity and geometry of concentrated and dilute solution channels should not be identical.

Acknowledgement

Financial support from ENERSENSE (Energy and Sensor Systems) group at Norwegian University of Science and Technology (NTNU) is greatly acknowledged. Zohreh Jalili would like to thank Dr. Vahid Alipour Tabrizy for all help and support throughout this work.

References

1. Yip N.Y., Brogioli D., Hamelers H.V.M., Nijmeijer K., *Environ. Sci. Technol.*, **50,** 12072-12094 (2016).
2. Vermaas D. A., Güler E., Saakes M., Nijmeijer K., *Energy Procedia*, **20,** 170-184 (2012).
3. Kingsbury R.S., Chu K., Coronell O. *J Memb Sci.*, **495,** 502-516 (2015).
4. Gurreri L., Tamburini A., Cipollina A., Micale G., Ciofalo M. *J Memb Sci.*, **468,** 133-148 (2014)
5. Gurreri L., Ciofalo M., Cipollina A., Tamburini A., Van Baak W., Micale G. *DESALIN WATER TREAT*, **55**(12), 3404-3423 (2015)
6. Schwinge J., Wiley D. E., Fletcher D. F. *Ind. Eng. Chem. Res.*, **41** (19), 4879-4888 (2002)
7. Ahmad A. L., Lau K. K., Bakar M. A. *J Memb Sci.*, **262** (1), 138-152 (2005).
8. Veerman, J. *University of Groningen*, **225,** (2010).
9. Vermaas D. A., Saakes M., Nijmeijer K. *J Memb Sci.*, **385,** 234-242 (2011).
10. Długołęcki, P., Dąbrowska J., Nijmeijer K., Wessling M. *J Memb Sci.*, **347** (1), 101-107 (2010).
11. Tadimeti J.G.D., Kurian, V., Chandra A., Chattopadhyay S.*J Memb Sci.*, **499,** 418-428 (2016).
12. Lacey R. E. *Ocean engineering*, **7** (1), 1-47 (1980).
13. Newman J., Thomas-Alyea K. E. *John Wiley and Sons*, (2012).
14. Kirby B. J. *Cambridge university press*, (2010).
15. Pawlowski S., Geraldes V., Crespo J.G., Velizarov S. *J Memb Sci.*, **502,** 179-190 (2016).
16. Ramon G. Z., Feinberg B. J., Hoek E. M. *Environ. Sci. Technol.*, **4** (11), 4423-4434 (2011).
17. Yip N. Y., Tiraferri A., Phillip W. A., Schiffman J. D., Hoover L. A., Kim Y. C., Elimelech M. *Environ. Sci. Technol.*, **45** (10), 4360-4369 (2011).
18. Rica R. A., Ziano R., Salerno D., Mantegazza F., van Roij R., Brogioli D. *Entropy*, **15** (4), 1388-1407 (2013).
19. Vermaas D. A., Veerman J., Yip N. Y., Elimelech M., Saakes M., Nijmeijer K. *ACS Sustain. Chem. Eng.*, **1** (10), 1295-1302 (2013).
20. OpenFOAM, The OpenFOAM Foundation, date of access: 09.01.2018, http://www.openfoam.org

21. swak4Foam, date of access: 01.05.2018, https://openfoamwiki.net/index.php/Contrib/swak4Foam
22. Sonin A. A., Probstein R. F. Desalination, **5** (3), 293-329 (1968).
23. Vermaas D. A., Saakes M., Nijmeijer K. *J Memb Sci.*, **453,** 12-319 (2014).
24. Sales B. B., Saakes M., Post J. W., Buisman C. J. N., Biesheuvel P. M., Hamelers H. V. M. *Environ. Sci. Technol.*, **44** (14), 5661-5665 (2010).
25. Hong J. G., Zhang B., Glabman S., Uzal N., Dou X., Zhang H., Chen Y. *J Memb Sci.*, **486,** 71-88 (2015).
26. Güler E., Elizen R., Vermaas D. A., Saakes M., Nijmeijer K. *J Memb Sci.*, **446,** 266-276 (2013).
27. Veerman J., Saakes M., Metz S. J., Harmsen G. J. *J. Appl. Electrochem.*, **40** (8), 1461-1474 (2010).
28. Zhu X., He W., Logan B. E. *J Memb Sci.*, **486,** 215-221 (2015).
29. Burheim O.S., F. Seland, J.G. Pharoah, S. Kjelstrup, *Desalination*, **285,** 147-152, (2012).
30. Burheim O.S., *Engineering Energy Storage*, Academic Press, **1st edition,** ISBN 9780128141007, (2017).

Nomenclature

A	Available membrane area
E_{OCP}	Open circuit potential
F	Faraday constant
I	Current
j	Current density
R	Universal gas constant
r_{AEM}	Ohmic area resistance of AEM
r_{CEM}	Ohmic area resistance of CEM
Re	Reynolds number
T	Temperature
H	Height of the channel
h_d	Heights of the dilute solutions compartments
L	Length of the channel
Δp	Pressure difference between inlet and outlet
ε	Spacer porosity
$\mathcal{D}_i$	Diffusivity

μ Dynamic viscosity

$\overline{\beta}$ Average perm-selectivity

ϕ Electrostatic potential

σ Mask fraction or spacer shadow factor

C Salt concentration of solution

C_c Concentration of the concentrated solution

C_d Concentrations of the dilute solution

D_c Corrugation diameter

H_c Height of the corrugation

h_c Heights of the concentrated solutions compartments

k_c Concentrated solution conductivity

k_d Dilute solution conductivity

L_i Length of inlet section

L_o Length of outlet section

L_{sp} Distance between the centre of two successive corrugations

N Number of corrugations

P_{RED}^{max} Maximum power density

$r_{unit\ cell}$ Unit cell resistance

u_{inlet} Velocity at inlet

z_i Valency